OPTO-ELECTRONICS REVIEW 9(2), 109–116 (2001)

Crystal growth of new functional materials for electro-optical applications♣

T. FUKUDA*, K. SHIMAMURA, A. YOSHIKAWA, and E.G. VÍLLORA

Institute for Materials Research, Tohoku University, 980–8577 Sendai, Japan

High quality fluoride and oxide single crystals for optical, piezoelectric, and other applications have been grown by advanced crystal growth techniques. Corquiriite- and Perovskite-type fluoride single crystals – $LiCaAlF_6$, $LiSrAlF_6$, $KMgF_3$ and $BaLiF_3$ – have been grown for solid state ultraviolet laser applications, and as window materials for next generation optical lithography. $La_3Nb_{0.5}Ga_{5.5}O_{14}$ and $La_3Ta_{0.5}Ga_{5.5}O_{14}$ piezoelectric single crystals of size and quality comparable to $La_3Ga_5SiO_{14}$ (langasite) have been produced. The piezoelectric and device properties of the crystals were investigated. A search for new langasite-type materials was also performed. Promising new structural materials, $Al_2O_3/RE_3Al_5O_{12}$ (RE = rare earth) eutectic fibres, have been grown by the micro-pulling-down technique. Undoped and doped ß-Ga_2O_3 single crystals have been grown by the floating zone technique as promising transparent conductive oxides.

Keywords: single crystals: $LiCaAlF_6$, $LiSrAlF_6$, $KMgF_3$, $BaLiF_3$, $La_3Nb_{0.5}Ga_{5.5}O_{14}$, $La_3Ta_{0.5}Ga_{5.5}O_{14}$; optical and piezoelectric properties.

1. Introduction

The important role of oxide and fluoride crystals in various branches of science and technology demands a comprehensive and integrated treatment of the subject. We have carried out investigations focusing on the development of new materials for optical, piezoelectric and other applications, using advanced crystal growth techniques. Oxide crystals are of highest importance for modern electrical and electro-optical applications in several devices. Fluoride single crystals, because of their unique properties such as large band gap, also present many advantages as optical materials.

The recent crystal growth research described in this work involved the development of new, high-quality oxide and fluoride single crystals, and of novel crystal growth techniques. The growth of fluoride single crystals doped with Ce for ultraviolet (UV) laser applications is reviewed. Growth of new langasite ($La_3Ga_5SiO_{14}$) single crystals for piezoelectric applications, by the Czochralski (CZ) technique, is discussed. The micro-pulling-down (μ-PD) method and its application to the growth of structural materials are mentioned. Crystal growth of ß-Ga_2O_3 for transparent conductive oxide (TCO) applications is also addressed.

2. Fluorides for UV optical applications

Coherent optical sources in the UV wavelength region are useful for many practical applications, such as medical procedures, semiconductor processing and remote sensing [1]. Recently, Ce-doped $LiCaAlF_6$ (Ce:LiCAF) and $LiSrAlF_6$ (Ce:LiSAF) single crystals have been reported as leading candidates for tunable all-solid- -state-lasers in the UV wavelength region [2,3]. However, due to the limited size of the available crystals, it was difficult to obtain high energy output directly from a Ce:LiCAF laser. Furthermore, the growth of Ce:LiCAF itself was known to be difficult [4].

Crystal growth was performed in a CZ system with a resistive heater made of high-purity graphite. The starting material was prepared from commercially available AlF_3, CaF_2, SrF_2, and LiF powders of high purity (>99.99%). The composition was 1 mol.% LiF and AlF_3 enriched from a stoichiometric one, in order to compensate for the vaporisation of LiF and AlF_3. As dopants, CeF_3 and NaF powders of high purity (>99.99%, Rare Metallic Co., Ltd.) were used. Na^+ was co-doped with Ce^{3+} in order to maintain the charge neutrality. The concentration of Ce^{3+} and Na^+ in the starting material was 1 mol.%. The pulling rate was 1 mm/h and the rotation rate was 10 rpm. Crystal growth was performed under high purity CF_4 gas (99.9999%).

Figure 1 shows as-grown Ce:LiCAF and Ce:LiSAF single crystals with dimensions of 18 mm in diameter and 60 mm in length. Cracks, bubbles and inclusions were not observed. Under the modified growth conditions, foreign substances on the surface of the grown crystal, as observed in Ref. 5, were not formed. However, Ce:LiSAF showed a tendency to crack perpendicular to the growth axis after several days. On the contrary, Ce:LiCAF did not show cracks at any time. Therefore, LiCAF was chosen for the

* e-mail: fukuda@lexus.imr.tohoku.ac.jp

♣ The paper presented there appears in SPIE Proceedings Vol. 4412 (2001).

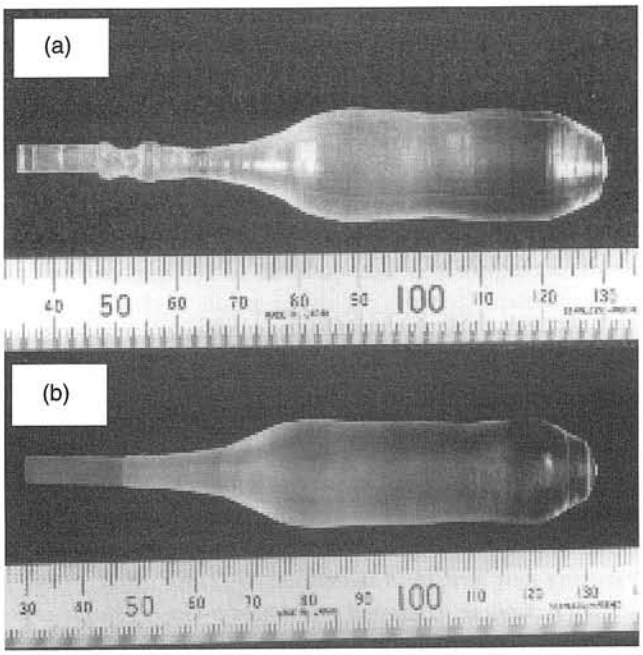

Fig. 1. As-grown Ce-doped $LiCaAlF_6$ (a) and $LiSrAlF_6$ (b) single crystals.

growth of large diameter crystals. The effective distribution coefficient (k_{eff}) of Ce^{3+} in LiCAF and LiSAF has been determined to be 0.021 and 0.013, respectively. The k_{eff} of Ce^{3+} in LiCAF was larger than in LiSAF. This is because the ionic radius of Ce^{3+} under 6-fold coordination (1.01 Å) is closer to that of Ca^{2+} (1.00 Å) than to that of Sr^{2+} (1.18 Å) [6], the ions thought to be replaced by Ce^{3+} [5].

Figure 2 shows an as-grown Ce:LiCAF single crystal of 2-inch diameter, free from cracks and inclusions. When crystals of this diameter were grown, the following two problems, not observed for crystals of 18-mm diameter, appeared: formation of inclusions, and cracks accompanied by the formation of an impurity phase at the bottom of the crystal.

Figure 3 shows a crystal which contains inclusions. It should be noticed that the formation of these inclusions was related to a change of the crystal diameter, for example at the shoulder part of the crystal. Once they appeared at the shoulder part, they did not disappear during crystal growth. In order to avoid these inclusions, the diameter at the shoulder part had to be controlled precisely and extended smoothly, without rapid change of the diameter. Although the absorption spectrum for the inclusion free region did not show any absorption peaks, that of the region with inclusions had one small absorption peak around 3600 cm^{-1}. Since this peak indicates the existence of OH-[1], it is thought that H_2O based impurities were present in the inclusions.

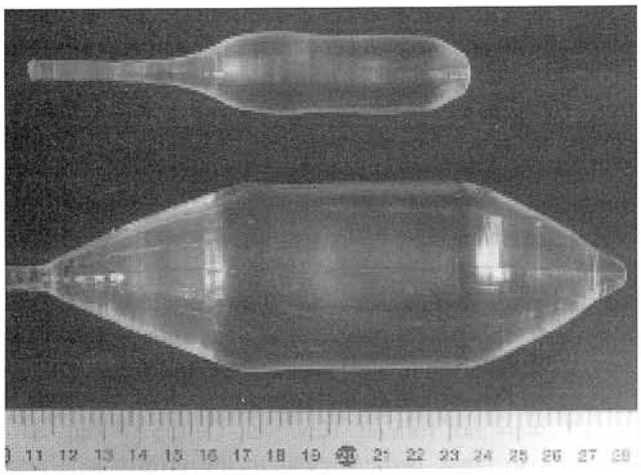

Fig. 2. 2-inch size Ce,Na:$LiCaAlF_6$ single crystal, compared with 1 inch crystal.

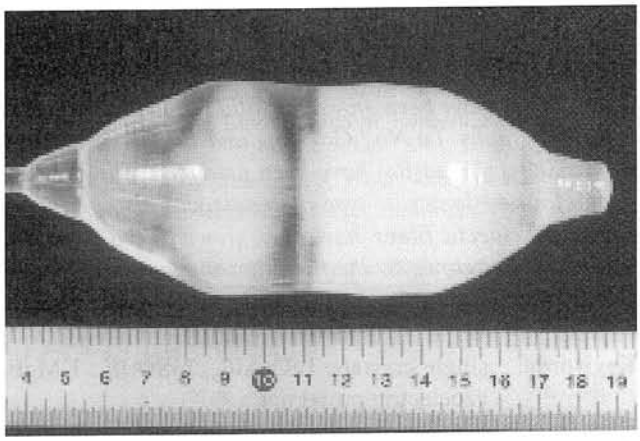

Fig. 3. Ce:$LiCaAlF_6$ crystal with inclusions.

Figure 4 shows an as-grown crystal with one large crack along the growth axis and a white substance at the bottom of the crystal. This large, flat crack appeared during cooling after growth, in cases when white material was present. This white substance usually formed when the solidification fraction exceeded 70%. The XRD analysis showed that the white substance was composed of LiCAF and CaF_2 phases. This is because the melt composition shifted in the CaF_2-enriched direction during growth, since the vaporisation pressure of LiF and AlF_3 is very high [7]. CeF_3 and NaF might have accumulated in the residual melt due to the small k_{eff}. In order to avoid formation of this white substance, crystal growth was terminated at the solidification fraction 60%, as for the crystal shown in Fig. 2.

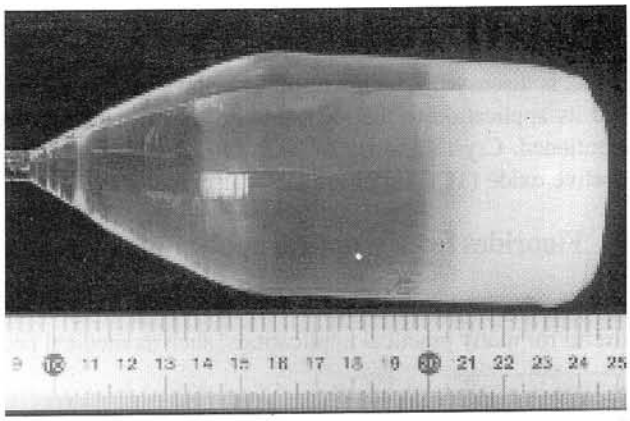

Fig. 4. Ce:$LiCaAlF_6$ crystal with white substances.

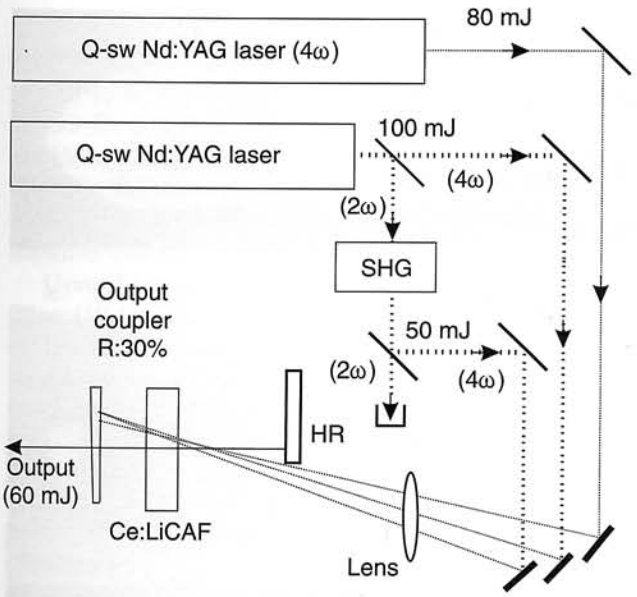

Fig. 5. Ce:$LiCaAlF_6$ laser setup.

For further improvement, optimisation of melt composition should be carried out.

We have already demonstrated an output energy of 30 mJ from a UV solid-state Ce:LiCAF laser that operated at 290 nm at a repetition rate of 10 Hz [5,8]. In order to obtain higher output energy, we increased the pumping energy. Figure 5 shows a setup for laser experiments. We obtained 60 mJ at 10 Hz, to our knowledge the highest performance so far reported for Ce:LiCAF.

Figure 6 shows the transmission edge of the LiCAF and LiSAF single crystals grown under Ar and CF_4 atmosphere. The transmission edge of LiCAF was measured to be at 112 nm and that of LiSAF – 116 nm, the shortest reported to our knowledge. The absorption at around 125 nm observed from the crystals grown under Ar atmosphere, disappeared when crystals were grown under CF_4 atmosphere. These transmission characteristics of LiCAF and LiSAF show their high potential as optical window materials in the UV and vacuum UV (VUV) wavelength region.

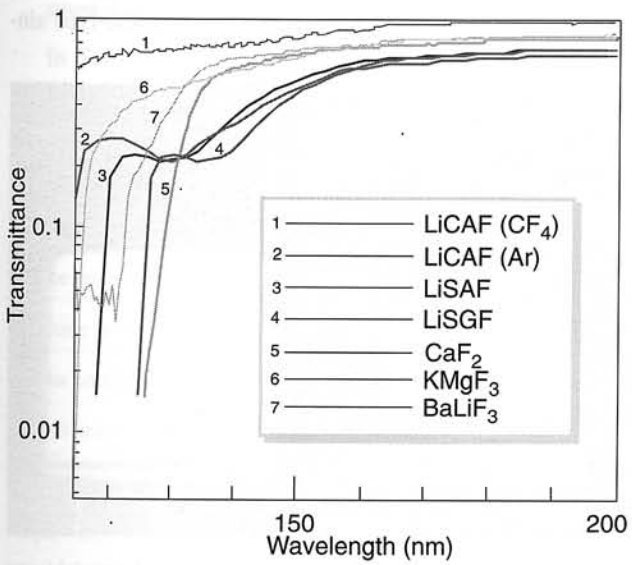

Fig. 6. Transmission spectra of different fluoride single crystals.

Recently, there has been significant interest in using 157-nm laser sources in projection lithography as successors to 193-nm based system. One of the most serious problems in realising a 157-nm based system is the development of suitable optical materials for lenses and other optical components. In particular, for an all-refractive design of 157-nm laser source, a second material other than CaF_2 is strongly required, because CaF_2 is the most promising material to be used. Primary candidates for a second material were LiF and MgF_2; however, they have several disadvantages such as a fragile and hydroscopic nature and large birefringence [9].

We have identified $KMgF_3$ (KMF) as a new promising optical material for 157-nm based system. The reasons to focus on KMF are as follows: (1) It belongs to the cubic crystal system [10], so theoretically it has no birefringence. (2) As it is composed of K and Mg cations, which have smaller atomic weight than Ca, it can be expected to have a shorter transmission edge than CaF_2. (3) As it melts congruently at a melting temperature of 1070°C [11], it can more likely be grown to a large size. $BaLiF_3$ (BLF) can also be a promising candidate, since it belongs to the cubic crystal system [12] and it can transmit 157-nm.

Crystal growth was performed in the same CZ system as for LiCAF and LiSAF. The starting material was prepared from commercially available high purity powders (>99.99%). The pulling rate was 0.5 to 1.5 mm/h and the rotation rate was 15 rpm.

Figure 7 shows an as-grown KMF and BLF single crystals 20 mm in diameter and 90 mm in length, pulled at a

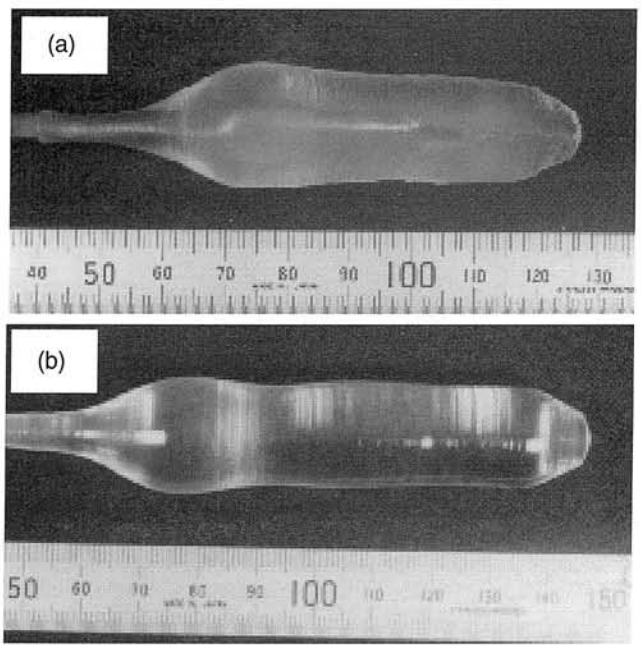

Fig. 7. $KMgF_3$ (a) and $BaLiF_3$ (b) single crystals.

rate of 1 mm/h. No cracks, bubbles or inclusions were observed. The thermal expansion coefficients of KMF and BLF along <111> was estimated to be 1.98×10^{-5} K^{-1} 3.06×10^{-5} K^{-1}, respectively, over the range 100–500°C. The variations of birefringence among KMF-wafer, BLF-wafer and LiCAF-wafer were of the order 10^{-7}, 10^{-5}, and 10^{-7}, respectively. Furthermore, the transmission edge of KMF and BLF single crystals was determined to be 115 nm and 120 nm. Figure 6 shows the transmission spectrum of KMF and BLF single crystals in VUV wavelength region, compared with LiCAF and LiSAF. The transmission characteristics of KMF and BLF single crystals shows its high potential as optical material in the UV and VUV wavelength region.

3. New langasite single crystals for piezoelectric applications

The recent progress of electronic technology requires new piezoelectric crystals having properties intermediate between those of quartz and $LiTaO_3$ (LT). Currently, langasite ($La_3Ga_5SiO_{14}$; LGS) crystals have received attention as new candidates for piezoelectric applications [13,14].

The LGS crystal has the $Ca_3Ga_2Ge_4O_{14}$-type structure with the space group P321. There are four kinds of cation sites in this structure, which can be described by the chemical formula, $A_3BC_3D_2O_{14}$. In this formula, A and B represent the decahedral (twisted Thomson cube) site coordinated by 8 oxygens, and the octahedral site coordinated by 6 oxygens, respectively. C and D represent tetrahedral sites coordinated by 4 oxygens. Different isovalent and aliovalent substitutions in a given structure are quite interesting in themselves, and could, perhaps, also result in useful structural and physical properties.

High-quality single crystals of LGS, and its aliovalent analogs $La_3Nb_{0.5}Ga_{5.5}O_{14}$ (LNG) and $La_3Ta_{0.5}Ga_{5.5}O_{14}$ (LTG), were grown by the conventional CZ technique [15]. Figure 8 shows the as-grown LTG single crystals of approximately 2 and 3 inches diameter. Pulling and rotation rates were 1mm/h and 10 rpm, respectively.

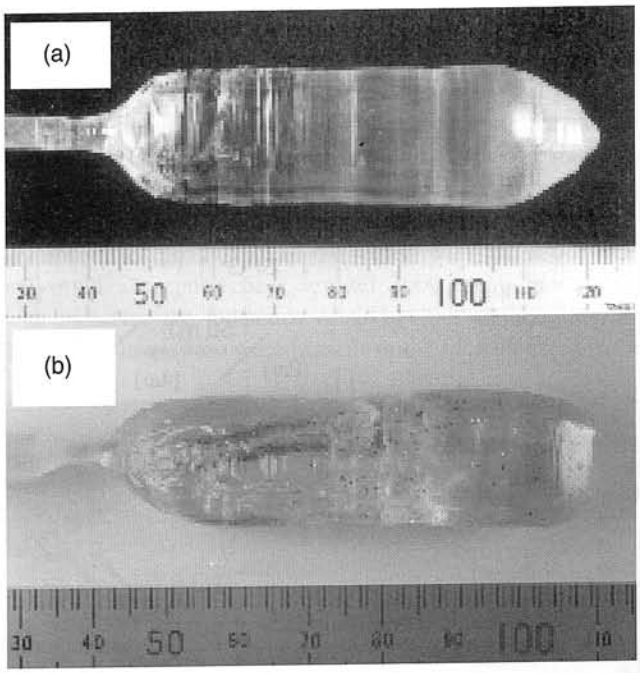

Fig. 9. $La_{3-x}Sr_xTa_{0.5+x/2}Ga_{5.5-x/2}O_{14}$, x = 0.1554 (a) and $Sr_3TaGa_3Si_2O_{14}$ (b) single crystals.

Lattice parameters of the grown crystals were found to be almost constant from shoulder to tail of the boules. Concentrations of each oxide, i.e., La_2O_3, Ga_2O_3, SiO_2, Nb_2O_5 and Ta_2O_5, were almost constant, within the estimated errors, throughout the crystallising process. The uniformity of lattice parameter and chemical composition suggests that the stoichiometric composition is close to the congruently melting composition of the three compounds.

Synthesis of more than 70 chemical compositions were attempted. The incorporation of different A cations (Na^+, Ba^{2+}, Sr^{2+}, Bi^{3+}, Nd^{3+}, etc) and B cations (Li^+, Mg^{2+}, Ga^{3+}, Ti^{4+}, Sb^{5+}, Mo^{6+}, etc) into the A and B sites was studied, respectively. Materials which showed a langasite-type sin-

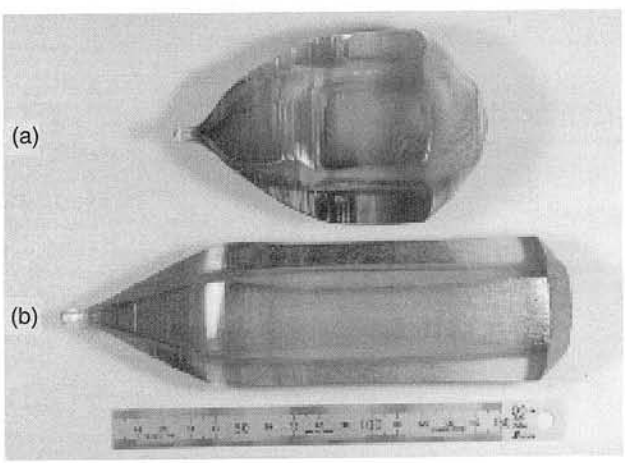

Fig. 8. $La_3Ta_{0.5}Ga_{5.5}O_{14}$ single crystals 3-inch (a) and 2-inch (b) diameter.

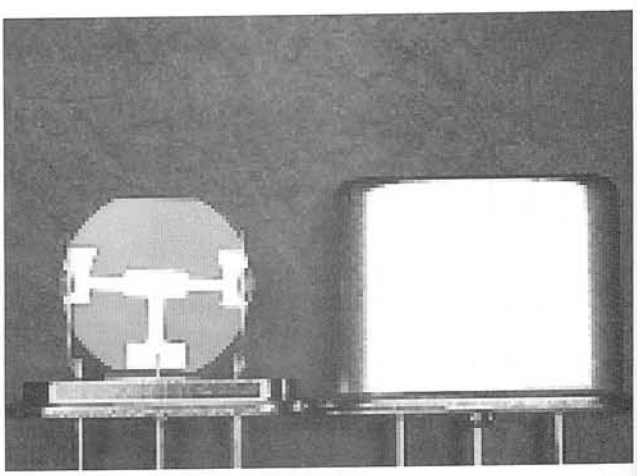

Fig. 10. 21.4 MHz filter made of $La_3Ga_5SiO_{14}$ single crystal (size: $6.9\times5.8\times2.2$ mm^3).

gle phase were crystallised in fibre form by the μ-PD method, and subsequently their bulk crystals were also grown by the Cz technique. Bulk single crystals of $Sr_3Ga_2Ge_4O_{14}$, $Na_2CaGe_6O_{14}$, $Pr_3Ga_5SiO_{14}$ and $La_3Al_xGa_{5-x}SiO_{14}$ were successfully produced by CZ technique. In Fig. 9, $La_{3-x}Sr_xTa_{0.5+x/2}Ga_{5.5-x/2}O_{14}$, x = 0.1554 (LSTG) and $Sr_3TaGa_3Si_2O_{14}$ (STGS) single crystals are shown as examples.

Using LGS single crystals, we made monolithic-type filters (10.4 and 21.4 MHz) as seen in Fig. 10. The electrical properties of these filters include low input and output impedance, small size and low attenuation, compared with those made of quartz (see Table 1).

Tab.1. Electrical properties of LGS monolithic type filters compared with quartz ones.

Frequency (MHz)	Material	Passband width (3dB) (kHz)	Attenuation (dB)	Input-output impedance (kΩ //pF)
10.7	Quartz	3 ±15	2.5	5.5k//1.0
	LGS	3 ±15	2.0	2.5k//1.7
21.4	Quartz	3 ±15	2.0	2.0k//0.5
	LGS	3 ±15	2.0	800//4.0
	LGS	3 ±15	2.0	1.3k//1.7

A 71 MHz-wide passband SMD (surface mount discrete-type) filter for the GSM (global system for mobile communication) base station was also made, which exhibited superior properties. The main features of the electrical characteristics are listed below:

- low input and output impedance (940Ω /0.5 pF, versus several kΩ for quartz filter),
- interstage coupling requires only capacitors (for quartz filter, transfer is required),
- electrode gap may be wide (approximately 100 mm, vs. several mm for quartz filter).

In Table 2, the characteristics of LNG, LTG and LGS are given, along with those of LT and quartz. Since LNG, LTG and LGS have no phase transitions and have lower melting point and higher hardness, the possibility of growing high-quality crystals allowing easy processing is expected to be likely. Their electromechanical coupling factors k and thermal frequency stability are between those of LT and quartz. The above characteristics indicate that LGS-family crystals are more promising materials for piezoelectric devices than lithium tetraborate ($Li_2B_4O_7$) and berlinite single crystals, which have similar piezoelectric properties [14]. $Li_2B_4O_7$ is easily soluble in all acids and bases, and easily deliquescent in air, while berlinite single crystals are difficult to grow to a large size.

Figure 11 shows the dependence of the electro-mechanical coupling factor, k_{12}, on the lattice parameter a in the langasite-type crystals. As can be seen from the figure, an increase in lattice parameter a leads to an increase of the electro-mechanical coupling factor, k_{12}. The electro-mechanical coupling factor of LTG is the largest of the langasite-type crystals studied. Therefore, we conclude that substitution of the B site is effective for improvement of the piezoelectric properties. This tendency serves as a guide for development of improved compounds of langasite-type structure.

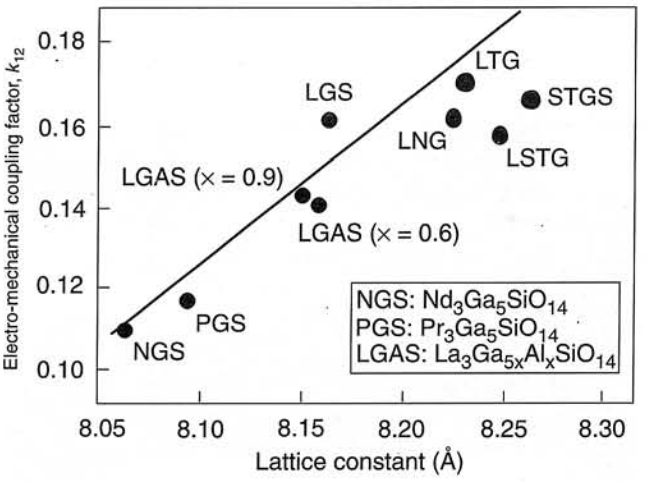

Fig. 11. Electro-mechanical coupling factor vs. lattice.

Tab. 2. Characteristics of LNG, LTG and LGS compared with those of LT and quartz.

	$LiTaO_3$	LGS	LNG	LTG	Quartz
Phase transition	exist	none	none	none	exist
Melting point (°C)	1650	1490	1470	1500	–
Mohs hardness	5.5	6~7	6~7	6~7	7
Electromechanical coupling factor *k* (%)	43	15~25	~30	~30	7
Q-factor	5000	30 000~40 000	40 000~60 000	40 000~60 000	60 000~80 000
Equivalent series resistance (Ω)	–	5~10	2~5	2~5	10~20
Thermal stability (ppm) (–20~70°C)	200~400	~150	~150	~150	10~20

4. Fibre crystals

Directionally solidified ceramic eutectics are drawing a strong interest because of their high structural stability up to the melting temperature. Recently, promising results were reported for $Al_2O_3/Y_3Al_5O_{12}$ (YAG) [16,18] and $Al_2O_3/GdAlO_3$ [19] systems. However, because of processing difficulties, the experimental data for oxide eutectics are still limited and often uncertain.

We have applied the μ-PD method for the growth of Al_2O_3/YAG eutectic fibres. The μ-PD method involves downward pulling of a crystalline fibre 0.1–2.0 mm in diameter through a capillary hole arranged in a crucible bottom. The μ-PD features two points important for eutectic growth:

- a very high axial temperature gradient exists near the growth interface of the order of $(3–5)\times10^3$°C/cm [20] (it permits high pulling rates and assures a planar interface and process stability).
- secondly, composition is always uniform along the fibre length, since melt convection is impossible inside the narrow capillary channel.

A high-temperature version of μ-PD employed an iridium crucible directly coupled to the RF power generator. A sapphire <0001> seed was used for growth of the eutectic fibres. The starting materials were 4N purity Al_2O_3 and Y_2O_3 in the molar ratio of 81.3 mol% Al_2O_3 to 18.7 mol% Y_2O_3 [21].

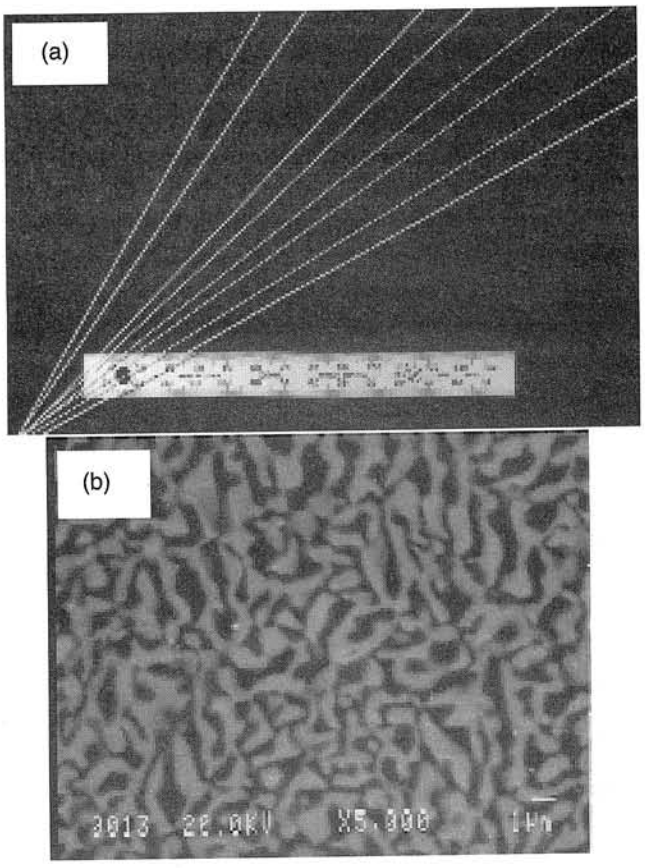

Fig. 12. Eutectic fibres (a) and back scattered electron image of $Al_2O_3/Y_3Al_5O_{12}$ fibres (b).

Eutectic fibres 0.25–1.00 mm in diameter and up to 500 mm in length were grown over a range of pulling rate 0.15–10.00 mm/min (see Fig. 12). Samples of eutectic fibres grown under various pulling rates were examined using scanning electron microscopy (SEM). Several fibres were grown at a step-variable pulling rate starting from 0.15 and up to 10 mm/min. In all these experiments, the "Chinese script" type structure was found to possess excellent reproducibility, whereas the cellular structure was not found at all. (The microstructure of eutectic sometimes forms the structure, which is resembles to Chinese character. Such microstructure is called "Chinese-script type" microstructure). The volume fraction of YAG was 0.45 ±0.02 for all types of structure including inter-cell areas, which corresponds exactly to the theoretical value for the eutectic composition (0.44). The characteristic script size was found to be very uniform for each cross-section studied. Experimentally, the generally accepted relation $\lambda \sim v_p^{-1/2}$ (where λ is interlamellar spacing of a conventional lamellar structure and v_p is the solidification rate) also applies to the script structure of the Al_2O_3/YAG system. The constant of proportionality was found to be 10, if λ has dimensions of mm and v_p mm per second. This value is large enough to allow effective microstructure control by changing solidification rate.

The composite has been shown to have high mechanical strength up to 1800°C, excellent oxidation resistance, high thermal stability of microstructure and thermal shock stability (Fig. 13). $Al_2O_3/Tm_3Al_5O_{12}$ showed a tensile strength of 620 MPa at 1500°C in vacuum. This is the highest strength at this temperature to date.

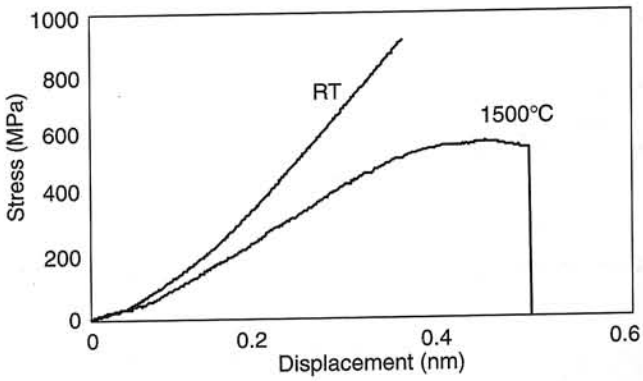

Fig. 13. Tensile stress-displacement curves of $Al_2O_3/Y_3Al_5O_{12}$ eutectic fibres (grown in Ar gas atmosphere).

5. ß-Ga_2O_3 as transparent conductive oxide

ß-Ga_2O_3 is transparent with a band gap of 4.8 eV, and belongs to the space group C2/m. It is intrinsically an insulator, but its n-type semiconduction when grown under reducing conditions is well known [22]. An undesired side effect is the resulting blue coloration, and thus degradation of the transmission, a fundamental property for window applications such as displays, solar cells, etc. Improvement of

electrical conductivity through the addition of dopants while preserving the transparency of the pure ß-Ga_2O_3 makes of this material a substitutive candidate for transparent conductive oxides (TCOs). Moreover, its shorter absorption edge will allow to extend the application fields of TCOs.

Powders of Ga_2O_3, WO_3 and HfO_2 of nominal 4N purity were mixed, sintered and grown to single crystals using the floating zone (FZ) technique with a double ellipsoid image furnace (ASGAL Co.:SS-10W). The growth was done under previously optimised conditions: growth rate of 5 mm/h, simultaneous rotation of feed and seed rods at 20 rpm in opposite directions, 500 ml/min. gas flow of different N_2/O_2 mixtures. The grown crystals had typical length of 3–4 cm, and diameter varying between 0.5 and 1 cm. For transmission and electrical measurements, crystals were cleaved in the (001) plane to obtain thin platelet-like samples, which exhibited flat, reflective surfaces.

The optical and electrical properties of the as-grown crystals depended on the concentration of the dopants and on the oxygen partial pressure. Crystal growth from nominally undoped feed rods under 1 atmosphere pressure was impossible due to the appearance and explosion of bubbles, which destabilised the molten zone. The formation of bubbles could be suppressed by the increase of pressure to 2 atmospheres (Fig. 14), or by the incorporation of W or Hf as dopants. Figures 15 and 16 show the crystals grown under

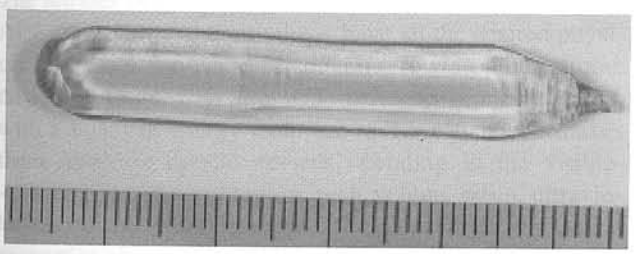

Fig. 14. Nominally pure ß-Ga_2O_3 single crystal grown under pure O_2 and a pressure of 2 atmosphere.

pure O_2 and 1 atmosphere pressure, with a nominal composition of the feed rod of 6 mol.% WO_3 and 0.2 mol.% HfO_2, respectively. These crystals were visually homogeneous, transparent, colourless and without cracks or inclusions. Improved transmittance and conductivity could be also achieved, indicating the beneficial effects of the substitution of Ga^{3+} by W^{4+} of Hf^{4+} and the potential optimisation of Ga_2O_3 properties for TCO applications.

6. Conclusions

Various new fluoride and oxide crystals were developed. Ce:LiCAF and Ce:LiSAF single crystals of 18 mm diameter were grown by the CZ technique under CF_4 atmosphere. Under the same growth conditions, Ce:LiCAF single crystals of 50 mm diameter (2 inches) were also grown up to a solidification fraction of 60%. Laser output energy of 60 mJ was obtained. This demonstrates that Ce:LiCAF is a promising material for high-energy UV pulse generation. KMF and BLF single crystals of 20-mm diameter were also grown. LiCAF, LiSAF, KMF and BLF single crystals showed a transmission edge at 112 nm, 119 nm, 115 nm and 120 nm, respectively. These characteristics indicate the high potential of these crystals as optical materials. A series of new promising langasite-type materials were found. LGS, LNG and LTG single crystals with maximum size of 3 inches in diameter were successfully grown by the Czochralski technique. Prototype models of wide passband filters were prepared using these crystals. LGS, LNG and LTG single crystals showed to have superior piezoelectric properties compared to other compounds with properties intermediate between those of quartz and LT. By applying the high-temperature µ-PD technique, directionally-solidified eutectic Al_2O_3/REAG fibres were grown. Al_2O_3/$Tm_3Al_5O_{12}$ showed a tensile strength of 620 MPa at 1500°C in vacuum. Undoped and doped ß-Ga_2O_3 single crystals were grown by the FZ technique. The substitution of Ga^{3+} by W^{4+} or Hf^{4+} improved transmittance and conductivity, indicating the potential optimisation of ß-Ga_2O_3 properties for TCO applications.

Acknowledgements

The authors would like to acknowledge and thank to Associate Professor Dr S. Durbin and the members of the Fukuda laboratory of the Institute for Materials Research, Tohoku University. They are also indebted to Mr J. Sato (TDK Corporation), Mr H. Kawanaka (Victor company of Japan, Ltd.), and Mr S. Murakami (KYOCERA Corporation) for their many contributions.

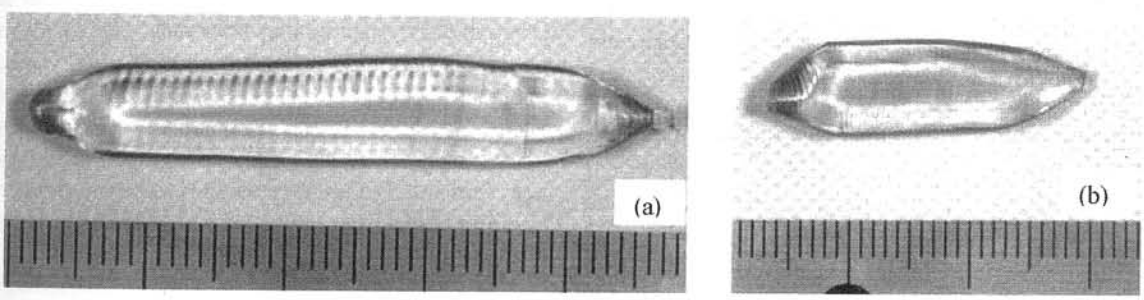

Fig. 15. W-doped (a) and Hf-doped (b) ß-Ga_2O_3 single crystals grown under pure O_2, 1atm pressure.

References

1. N. Sarukura, M.A. Dubinskii, Z. Liu, V.V. Semashko, A.K. Naumov, S.L. Korableva, R.Y. Abdulsabirov, K. Edamatsu, Y. Suzuki, T. Itoh, and Y. Segawa, *IEEE J. Selected Topics in Quantum Electronics* **1**, 792 (1995).
2. M.A. Dubinskii, V.V. Semashko, A.K. Naumov, R.Y. Abdulsabirov, and S.L. Korableva, *Laser Phys.* **3**, 216 (1993).
3. C.D. Marshall, S.A. Payne, J.A. Speth, W.F. Krupke, G.J. Quarles, V. Castillo, and B.H.T. Chai, *J. Opt. Soc. Am.* **B11**, 2054 (1994).
4. R.F. Belt and R. Uhrin, *J. Cryst. Growth* **109**, 340 (1991).
5. K. Shimamura, N. Mujilatu, K. Nakano, S.L. Baldochi, Z. Liu, H. Ohtake, N. Sarukura, and T. Fukuda, *J. Cryst. Growth* **197**, 896 (1999).
6. R.D. Shannon, *Acta Cryst.* **A32**, 751 (1976).
7. D. Klimm and P. Reiche, *Proc. Int. Symp. Laser and Nonlinear Optical Materials*, 3–5 November, 284 (1997).
8. Z. Liu, S. Izumida, H. Ohtake, N. Sarukura, K. Shimamura, N. Mujilatu, S.L. Baldochi, and T. Fukuda, *Jpn. J. Appl. Phys.* **37**, L1318 (1998).
9. T.M. Bloomstein, M.W. Hom, M. Rothschild, R.R. Kunz, S.T. Palmacol, and R.B. Goodman, *J. Vac. Sci. Technol.* **B15**, 2112 (1997).
10. A. Darabont, C. Neamtu, S.I. Farcas, and G. Borodi, *J. Cryst. Growth* **169**, 89 (1996).
11. R.C. DeVries and R. Roy, *J. Am. Chem. Soc.* **75**, 2481 (1953).
12. S.L. Baldochi, K. Shimamura, K. Nakano, N. Mujilatu, and T. Fukuda, *J. Cryst. Growth* **200**, 521 (1999).
13. I.M. Silvestrova, Yu.V. Pisarevsky, V.V. Bezdelkin, and P.A. Senyushenkov, *Proc. 1993 IEEE International Frequency Control Symposium*, p. 351.
14. J. Detaint, J. Schwartzel, A. Zarka, B. Capelle, J.P. Denis, E. Philippot, *Proc. IEEE International Frequency Control Symposium*, 58 (1994).
15. K. Shimamura, H. Takeda, T. Kohno, and T. Fukuda, *J. Cryst. Growth* **163**, 388 (1996).
16. T.A. Parthasarathy, T.I. Mah, and L.E. Matson, *J. Am. Ceram. Sci.* **76**, 29 (1993).
17. Y. Waku, N. Nakagawa, H. Ohtsubo, Y. Ohsora, and Y. Kohtoku, *J. Jpn. Inst. Metals* **59**, 71 (1995).
18. Y. Waku, H. Ohtsubo, N. Nakagawa, and Y. Kohtoku, *J. Mater. Sci.* **31**, 4663 (1996).
19. Y. Waku, N. Nakagawa, T. Wakamoto, H. Ohtsubo, K. Shimizu, and Y. Kohtoku, *Nature* **389**, 49 (1997).
20. S. Uda, J. Kon, J. Ichikawa, K. Inaba, K. Shimamura, and T. Fukuda, *J. Cryst. Growth*, **179**, 567 (1997).
21. D. Viechnicki and F. Schmid, *J. Mater. Sci.* **4**, 84 (1969).
22. N. Ueda, H. Hosono, R. Waseda, and H. Kawazoe, *Appl. Phys. Lett.* **70**, 3591 (1997).

